[redacted]

NASA TECHNICAL MEMORANDUM

NASA TM X-1404

NASA TM X-1404

AN EXPERIMENTAL AERODYNAMIC HEATING STUDY OF A VARIABLE-GEOMETRY LIFTING-BODY REENTRY CONFIGURATION

by Irving Weinstein and Bernard Spencer, Jr.

[redacted]

Langley Research Center
Langley Station, Hampton, Va.

NATIONAL AERONAUTICS AND SPACE ADMINISTRATION • WASHINGTON, D. C. • JUNE 1967

[redacted]

[redacted] NASA TM X-1404

AN EXPERIMENTAL AERODYNAMIC HEATING STUDY OF A VARIABLE-GEOMETRY LIFTING-BODY REENTRY CONFIGURATION

By Irving Weinstein and Bernard Spencer, Jr.

Langley Research Center
Langley Station, Hampton, Va.

[redacted]

[redacted]

[redacted]

[redacted]

NATIONAL AERONAUTICS AND SPACE ADMINISTRATION

[redacted]

AN EXPERIMENTAL AERODYNAMIC HEATING STUDY OF A VARIABLE-GEOMETRY LIFTING-BODY REENTRY CONFIGURATION*

By Irving Weinstein and Bernard Spencer, Jr.
Langley Research Center

SUMMARY

An investigation was made to study experimentally the aerodynamic heating effects on the various components of a variable-geometry lifting-body reentry vehicle. The tests were conducted in a flow medium of methane-air combustion products at a nominal Mach number of 7.0, at total temperatures from 3140° R to 3440° R (1740° K to 1910° K), and at free-stream Reynolds numbers of approximately 0.8×10^6 and 1.7×10^6 per foot (2.6 and 5.6 per μm).

Heating contours obtained over the surfaces of the models provide indications of heat-load distribution as well as the areas of highest heating. The region near the leading edges of the horizontal-tails at -30° and -60° dihedral experiences a high heating rate and would be of prime concern in a final vehicle design. For a given angle of attack, a reduction in incidence on the -30° dihedral tails reduces the heating level somewhat over the surfaces as would be expected.

INTRODUCTION

The National Aeronautics and Space Administration is presently engaged in studies to determine the aerodynamic characteristics of lifting-body spacecraft configurations over the low subsonic to hypersonic speed range. The present configuration combines a hypersonic lift-drag ratio of approximately 2 and good horizontal landing characteristics by use of variable-sweep wings. (See refs. 1 to 4.) The configuration concept consists of an elliptic-cross-section hypersonic minimum-wave-drag body as determined by methods described in reference 5 and modified by the addition of low-mounted horizontal tails and variable-sweep wing panels. Although the low-mounted horizontal tails have been found to provide good stability and control characteristics throughout the speed ranges of the tests, consideration of the aerodynamic heating problem during reentry and

*Title, Unclassified.

at hypersonic speeds could dictate the feasibility of employing these tails in the low-mounted location. For this reason, an investigation has been conducted to examine, qualitatively, some of the effects of aerodynamic heat flux to the basic body for conditions with and without nose bluntness and for the horizontal tails at various dihedral and incidence angles. These studies have been made at two angles of attack (15° and 37.5°) corresponding approximately to that for maximum lift-drag ratio and for near-maximum lift coefficient, respectively.

The tests were conducted in the 7-inch (18-cm) Mach 7 pilot tunnel at the Langley Research Center. This tunnel uses the combustion products of methane and air as the test medium. The data were obtained at a nominal Mach number of 7, at total temperatures from 3140° R to 3440° R (1740°K to 1910° K), and at free-stream Reynolds numbers of approximately 0.8×10^6 and 1.7×10^6 per foot (2.6 and 5.6 per μm).

SYMBOLS

The units used for the physical quantities in this paper are given both in the U.S. Customary Units and in the International System of Units (SI). Factors relating the two systems are given in reference 6 and those used in the present investigation are presented in the appendix.

i_h	horizontal-tail incidence angle (positive with trailing edge down), deg
l	model reference length (see fig. 1)
M	free-stream Mach number
p_t	model total pressure, psia $\left(N/m^2\right)$
$\dot{q}$	heat-transfer rate, Btu/ft^2-sec $\left(W/m^2\right)$
r	radius, in. (cm)
R	free-stream Reynolds number per foot (per μm)
T	temperature, $^{\circ}$R ($^{\circ}$K)
x	length measured along model center line from theoretical body nose (see fig. 1)

α angle of attack, deg

Γ_h horizontal-tail dihedral angle, deg

Λ wing half-chord sweep angle, deg

Subscripts:

eq equilibrium

ref reference

t total

MODELS, APPARATUS, AND PROCEDURES

Models

The model and components of the variable-geometry vehicle used for these tests are shown in figure 1, and the configurations tested are indicated in table I. The models had a maximum span across the -30° dihedral tails of 1.68 inches (4.27 cm) and had a length of 3.75 inches (9.52 cm) for the sharp-nose model. The blunted model had a nose radius of 0.11 inch (0.28 cm) in the horizontal plane and 0.05 inch (0.13 cm) in the vertical plane. The sharp-nose model actually had a radius of approximately 0.025 inch (0.064 cm). The wing panels are shown in both the 75° sweep and the fully retracted positions on the drawing of figure 1.

The models were cast from a ceramic material composed of 99.8 percent fused silica with the major impurity being aluminum oxide Al_2O_3 . Use of this material provides a rapid approach to surface equilibrium temperatures owing to its low thermal conductivity. The fabrication techniques used and the characteristics of this material are discussed in reference 7.

A photograph of several representative configurations is shown in figure 2. The models are shown painted with a black heat-resistant enamel and appear in the pre-test condition. The purpose of the paint is discussed in a subsequent section of this paper.

Apparatus

Tunnel.- The tests were conducted in the 7-inch (18-cm) Mach 7 pilot tunnel at the Langley Research Center. This facility is a hypersonic blowdown tunnel which attains a high thermal-energy level by burning a mixture of methane and air under high pressure.

The combustion products, which serve as a test medium, are expanded through an axisymmetric nozzle and through a free-jet test section. Drawings and a more detailed description of this facility may be found in references 8 and 9. Thermal and transport properties for the combustion products of methane and air are presented in reference 10.

Instrumentation.- A photographic pyrometer system was used to obtain the temperatures over the model surfaces. This system records the temperatures by exposing a photographic emulsion to the visible radiation from the incandescent surfaces of the model. The film negative will produce a high density in the region of high temperatures (i.e., high luminosity) and a lower density in the regions of lower temperature. The surface temperature was related to the image density through a calibration procedure in which a tungsten-lamp filament of known temperature and emissivity was photographed. An investigation and calibration of this technique are presented in reference 11 and the background theory and operation of a similar system are discussed in reference 12. The film densities were measured with a densitometer using an enlarger to project the image from the film to increase the area resolution. A discussion of the sources of error and the effects of material emissivity is presented in reference 7.

A single-pass, Z-type schlieren system was used to obtain shock patterns around the models. A continuous light source was used and photographs were obtained during the first part of each test run at a frame rate of 10 per second.

Test Procedure

During each test run, the tunnel equilibrium conditions were established before the model was inserted into the stream. The angle of attack and orientation of the model to the various cameras were set prior to exposure of the model to the flow. The alinement of the model support and the orientation of the model to give the required photographic view left a small inherent yaw angle for some of the test conditions. The model was exposed to the test stream for approximately 40 seconds to allow the heated surfaces to attain approximately equilibrium temperatures. Schlieren photographs were obtained during the first 10 seconds, after which the continuous light source was turned off and photometer pictures were obtained at 6-second intervals during the remainder of the test run. The photometer pictures were obtained in total darkness to insure that the light energy produced on the negative came entirely from the model heating. A black heat-resistant enamel was used on the model surfaces during the last phase of the tests (configurations 7 and 8). The glow from the small highly heated tail surfaces was reflected into the camera from the surrounding surfaces and was observed as heat by the photometer. The use of the black enamel greatly reduced the surface reflectivity in this region.

The tests were run at a nominal Mach number of 7, at free-stream total temperatures from 3140° R to 3440° R (1740° K to 1910° K), and at free-stream Reynolds

numbers of approximately 0.8×10^6 and 1.7×10^6 per foot (2.6 and 5.6 per μm). The models were tested at angles of attack of approximately 15° and 37.5°. Table I presents a summary of the pertinent test conditions and the corresponding model configurations for the test runs on the variable-geometry reentry vehicle.

Accuracy

The accuracy of the test conditions is as follows:

Angle of attack, α, deg	±0.3
Free-stream Mach number, M	±0.07
Temperature, T, $^\circ$R ($^\circ$K)	±25
Model total pressure, p_t, percent	±2

DATA REDUCTION

The data are presented in the form of nondimensional heating contours based on a thermal-heat balance at equilibrium conditions neglecting the conduction effects as described in reference 7. With the assumption that the emissivity over the model surface remains constant over the visual temperature range considered, the nondimensional heating ratio can be reduced to

$$\frac{\dot{q}}{\dot{q}_{ref}} = \left[\left(\frac{T}{T_{ref}}\right)_{eq}\right]^4$$

The data were nondimensionalized to a reference location along the lower surface center line. The photometer could not be located in a position to determine the stagnation-point temperature; therefore, any attempt to reference the data to this point would be based on the computed value. The computed value would induce an error based on the accuracy with which the total temperature could be determined. The error would be further increased when a ratio based on this computed value was raised to the fourth power. Any error could be greatly reduced by presenting the local temperature as a function of the temperature at a reference point, which is also determined photographically, since the error would be of the same order and in the same direction in both the numerator and denominator. The reference point was taken on the model at a location which heated to the visible range for all tests and was easily viewed by the photometer. This point was located along the lower surface center line at a distance of $0.24l$ aft of the theoretical body nose. The photometer records the light energy produced in the visible portion of the spectrum and therefore limits the readout temperatures to those above approximately 1500° F (1100° K). The heating contours of lowest value in the figures correspond to a value near the minimum readout temperature.

RESULTS AND DISCUSSION

Figure 3 presents the nondimensional heating contours obtained on the various configurations of the variable-geometry reentry model. Figure 3(a) presents the effects of Reynolds number for the sharp-nose basic-body configuration without tails at an angle of attack of 15°. A comparison of the heating over the lower surface at two different Reynolds numbers indicates that the absolute temperature at a given location on the surface is greater for the higher Reynolds number. There is no significant effect of heating-rate distribution, however, along the model – probably owing to the fact that for the small models the flow is laminar and there is no boundary-layer transition.

Figure 3(b) shows the effect of nose bluntness for the body without tails at an angle of attack of 15° at constant Reynolds number. The heating near the nose of the sharp model is greater than that for the blunt model at a corresponding location; however, at a short distance aft of the nose the heating rates on the two models are about the same.

The effects induced by the horizontal tails are shown in figure 3(c) for the sharp-nose body. The addition of horizontal tails produces an interfering flow field at the tail-body juncture which results in increased heating over the aft portion of the body. Although the nondimensional heating near the tail leading edges is not as great as that near the nose of the body, it is nevertheless quite high and would be a source of concern in a vehicle design. The effect of tail incidence, shown in figure 3(d), can be seen to produce higher heating values over the tails at 0° incidence than at -10° incidence. This result is as would be expected and is caused by the greater exposure to the flow for a given angle of attack.

The effect of wing sweep on the heating is shown in figure 3(e). The heating on the lower surface of the 75° swept wings is on the same order as that along the lower surface of the fuselage. This heating level on the wing is slightly lower than that experienced over the lower surface of the tails. Any nonsymmetry of the heating contours is due to either a small yaw angle inherent in some of the models or a nonuniform temperature distribution across the test region.

The effect of angle of attack on the heating is shown by the contours of figure 3(f) for a tail dihedral of -30° at angles of attack of 15° and 37.5°; these angles of attack were selected since they represent the angle near maximum lift-drag ratio and the angle near maximum lift, respectively. The heating-rate ratio is greater over the entire surface at the higher angle of attack. This configuration was tested with a center vertical tail as shown in figure 1. The vertical tail did not experience heating within the operational temperature range of the photographic pyrometer for either angle of attack of the tests. Figure 3(g) shows a similar comparison of the heating on a configuration having a tail dihedral of -60°. The heating contours seem to be about the same as those for the

configuration with a -30° tail dihedral angle. The upper surface of one of the horizontal tails in this figure was obscured from view of the camera and the contours are therefore not shown.

Curves of heating-rate ratio along the lower surface center line for two model configurations are shown in figure 4. It can be seen that there is very little change in the nondimensional heating due to an increase in Reynolds number since the flow is still laminar, as was pointed out in the discussion of figure 3(a). An increase in angle of attack resulted in an increased heating rate over most of the exposed surfaces. The fact that the curves cross at $\frac{\dot{q}}{\dot{q}_{ref}} = 1.0$ is a characteristic of the reference location and does not represent a change due to heating.

Schlieren photographs were taken of the various configurations, and typical views of the models are presented in figure 5. The side views are shown in figure 5(a) for an angle of attack of 15°. The shock waves produced by the tails of configuration 4 appear weaker than those for configuration 3 and are deflected less. This reduction in wave strength is attributed to the negative tail incidence for these two configurations. This result is also detected on the heating contours of figure 3 for these configurations. Figure 5(b) shows the flow around the models for different views at angles of attack of 15° and 37.5°. The metal adapter coming out of the model was wrapped with an asbestos tape at the high angle of attack as protection from the hot flow and shows up as a luminous area at the base of the model on the photographs. The side view for configuration 7 shows that the body shields the center vertical tail from the flow. Although this shielding protects the center vertical tail from high heating, it renders the tail ineffective for control purposes, particularly at the high angle of attack. The rolled views for configuration 8, which were photographed perpendicular to one of the horizontal tails, show that the bow shock hits the tip of the tails at $\alpha = 15°$ and crosses the tails at $\alpha = 37.5°$.

CONCLUDING REMARKS

Aerodynamic heating studies of several configurations of a variable-geometry reentry-vehicle model have been conducted in the 7-inch (18 cm) Mach 7 pilot tunnel at the Langley Research Center. Data were obtained at total temperatures from 3140° R to 3440° R (1740° K to 1910° K) and at free-stream Reynolds numbers of approximately 0.8×10^6 and 1.7×10^6 per foot (2.6 and 5.6 per μm).

In general, the heating contours obtained give an indication of the heating over the model surfaces and depict the areas of highest heating. The lower surfaces near the leading edges of the horizontal tails at -30° and -60° dihedral would be subjected to a high heating rate and would be of prime concern in a final vehicle design. For a given angle of attack, a reduction in incidence from 0° to -10° on the -30° dihedral tails reduces

the heating level somewhat over the surfaces, as would be expected. A center vertical tail added to the vehicle was shielded from the free-stream flow by the body itself at the test angles of attack and kept the heating level below that which could be determined by the method used.

Langley Research Center,
National Aeronautics and Space Administration,
Langley Station, Hampton, Va., February 8, 1967,
124-07-02-01-23.

APPENDIX

CONVERSION OF U.S. CUSTOMARY UNITS TO SI UNITS

The International System of Units (SI) was adopted by the Eleventh General Conference on Weights and Measures, Paris, October 1960, in Resolution No. 12 (ref. 6). Conversion factors for the units used herein are given in the following table:

Physical quantity	U.S. Customary Unit	Conversion factor (*)	SI Unit (**)
Heat-transfer rate. . .	Btu/ft^2-sec	11350	watts/meter^2 (W/m^2)
Length	in.	0.0254	meters (m)
Pressure.	psia	6895	newtons/meter^2 (N/m^2)
Reynolds number . . .	per ft	3.28	per meter (per m)
Temperature.	^oR	5/9	degrees Kelvin (^oK)

*Multiply value given in U.S. Customary Units by conversion factor to obtain equivalent value in SI Units.

**Prefixes to indicate multiple of units are as follows:

Prefix	Multiple
kilo (k)	10^3
centi (c)	10^{-2}
micro (μ)	10^{-6}

REFERENCES

1. Putnam, Lawrence E.: Hypersonic Aerodynamic Characteristics of a Reentry Configuration With Variable-Sweep Wings. NASA TM X-965, 1964.

2. Spencer, Bernard, Jr.; and Trescot, Charles D., Jr.: Effects of Reynolds Number at Low Subsonic Speeds on Aerodynamic Characteristics of a Reentry Body With a Variable-Sweep Wing. NASA TM X-1010, 1964.

3. Foster, Gerald V.; Fournier, Roger H.; and Spencer, Bernard, Jr.: Static Aerodynamic Characteristics at Mach Numbers From 1.50 to 4.63 of a Lifting Entry Configuration Having Variable-Sweep Wings. NASA TM X-1064, 1965.

4. Fournier, Roger H.; and Spencer, Bernard, Jr.: Aerodynamic Characteristics at Mach Numbers From 1.50 to 4.63 of a Variable-Geometry Lifting Reentry Concept Employing Elevators and Body Base Flaps for Control. NASA TM X-1351, 1967.

5. Suddath, Jerrold H.; and Oehman, Waldo I.: Minimum Drag Bodies With Cross-Sectional Ellipticity. NASA TN D-2432, 1964.

6. Mechtly, E. A.: The International System of Units – Physical Constants and Conversion Factors. NASA SP-7012, 1964.

7. Weinstein, Irving; and Howell, Robert R.: Technique for Measuring High-Temperature Isotherm Patterns on Aerodynamically Heated Models With Experimental Results. NASA TN D-2769, 1965.

8. Weinstein, Irving: Heat Transfer and Pressure Distributions on a Hemisphere-Cylinder and a Bluff-Afterbody Model in Methane-Air Combustion Products and in Air. NASA TN D-1503, 1962.

9. Schaefer, William T., Jr.: Characteristics of Major Active Wind Tunnels at the Langley Research Center. NASA TM X-1130, 1965.

10. Leyhe, E. W.; and Howell, R. R.: Calculation Procedure for Thermodynamic, Transport, and Flow Properties of the Combustion Products of a Hydrocarbon Fuel Mixture Burned in Air With Results for Ethylene-Air and Methane-Air Mixtures. NASA TN D-914, 1962.

11. Siviter, James H., Jr.; and Strass, H. Kurt: An Investigation of a Photographic Technique of Measuring High Surface Temperatures. NASA TN D-617, 1960.

12. Exton, Reginald J.: Theory and Operation of a Variable Exposure Photographic Pyrometer Over the Temperature Range 1800° to 3600° F (1255° to 2255° K). NASA TN D-2660, 1965.

TABLE I.- MODEL CONFIGURATIONS AND PERTINENT TEST CONDITIONS

Model configuration					Test conditions									
Model configuration	Nose shape	Λ, deg	Γ_h, deg	i_h, deg	Mode total pressure, p_t		Total temperature, T_t		M	Reynolds number, R		α, deg	Reference temperature, T_{ref}	
					psia	kN/m^2	^oR	^oK		per ft	per μm		^oR	^oK
1	Sharp	90			9.34	64.4	3280	1822	7.16	0.86×10^6	2.82	15.0	2140	1189
1	Sharp	90			16.90	116.5	3260	1811	7.27	1.69	5.54	15.0	2250	1250
2	Sharp	90	-30	0	9.40	64.8	3310	1839	7.14	.86	2.82	15.0	2125	1181
3	Sharp	75	-30	0	9.50	65.5	3350	1861	7.10	.83	2.72	15.0	2160	1200
4	Sharp	90	-30	-10	9.23	63.6	3230	1794	7.21	.89	2.92	15.0	2160	1200
5	Blunt	90			9.00	62.1	3140	1744	7.29	.93	3.05	15.0	2105	1169
6	Blunt	75			9.60	66.2	3390	1883	7.07	.82	2.69	15.0	2185	1214
*7	Blunt	90	-30	-10	9.05	62.4	3400	1889	7.07	.76	2.49	15.0	2320	1289
*7	Blunt	90	-30	-10	9.24	63.7	3440	1911	7.04	.77	2.53	37.5	2375	1319
8	Blunt	90	-60	0	8.27	57.0	3200	1778	7.23	.80	2.62	15.0	2220	1233
8	Blunt	90	-60	0	8.50	58.6	3160	1756	7.27	.86	2.82	37.5	2305	1281

*Center vertical tail on.

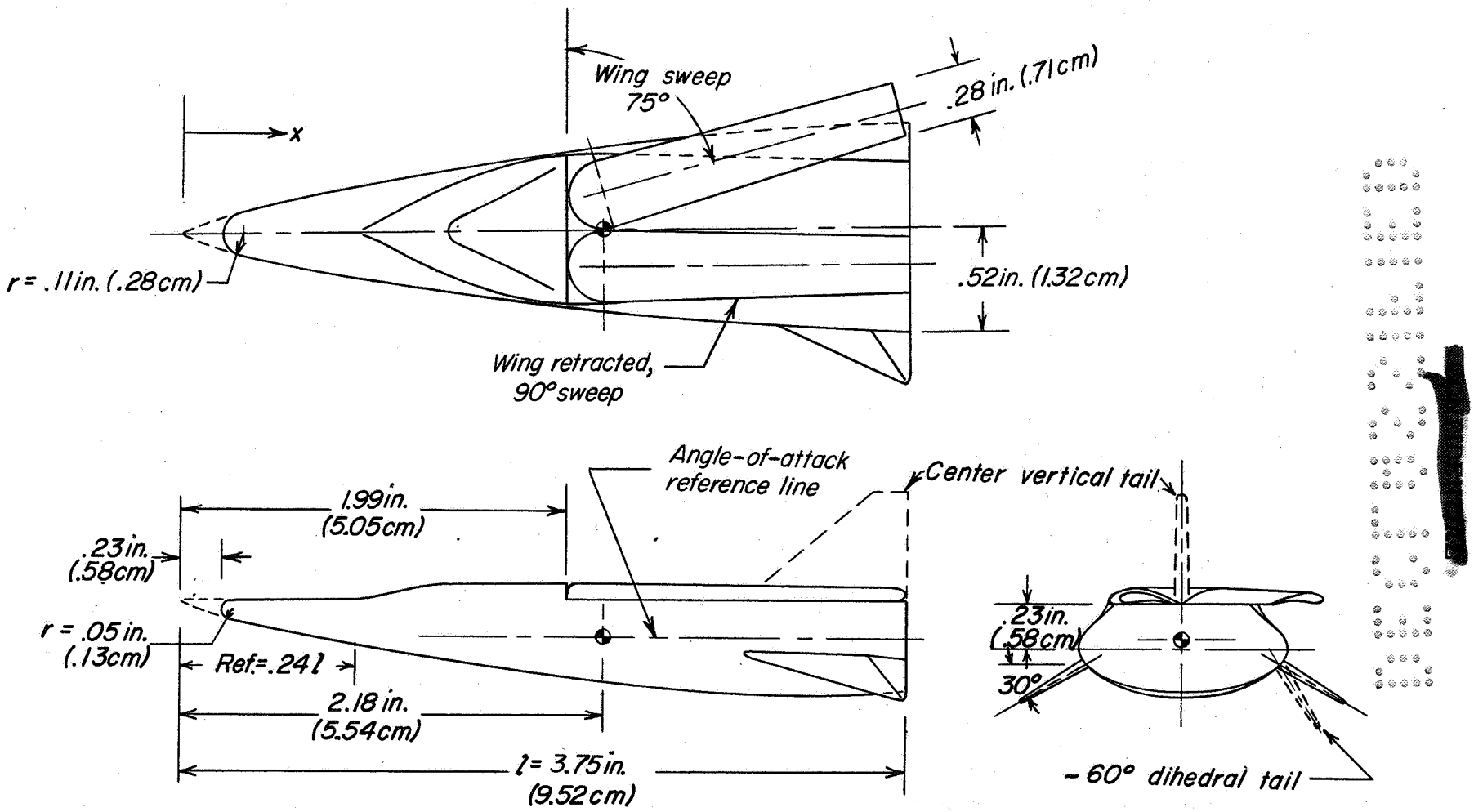

Figure 1.- Drawing and pertinent dimensions of variable-geometry vehicle. (Dimensions shown are model size.)

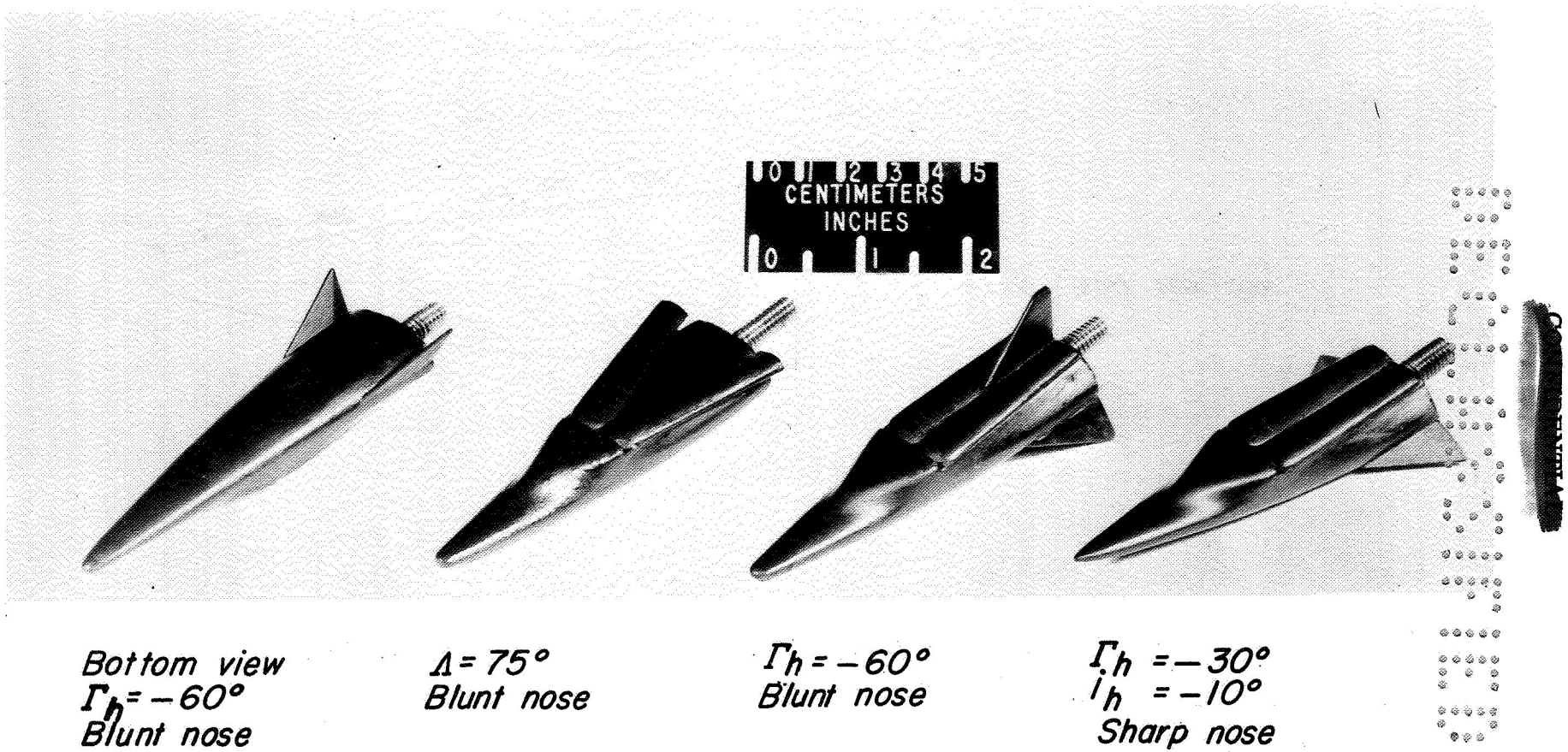

L-67-1010

Figure 2.- Photograph of several ceramic-model configurations of a variable-geometry reentry vehicle.

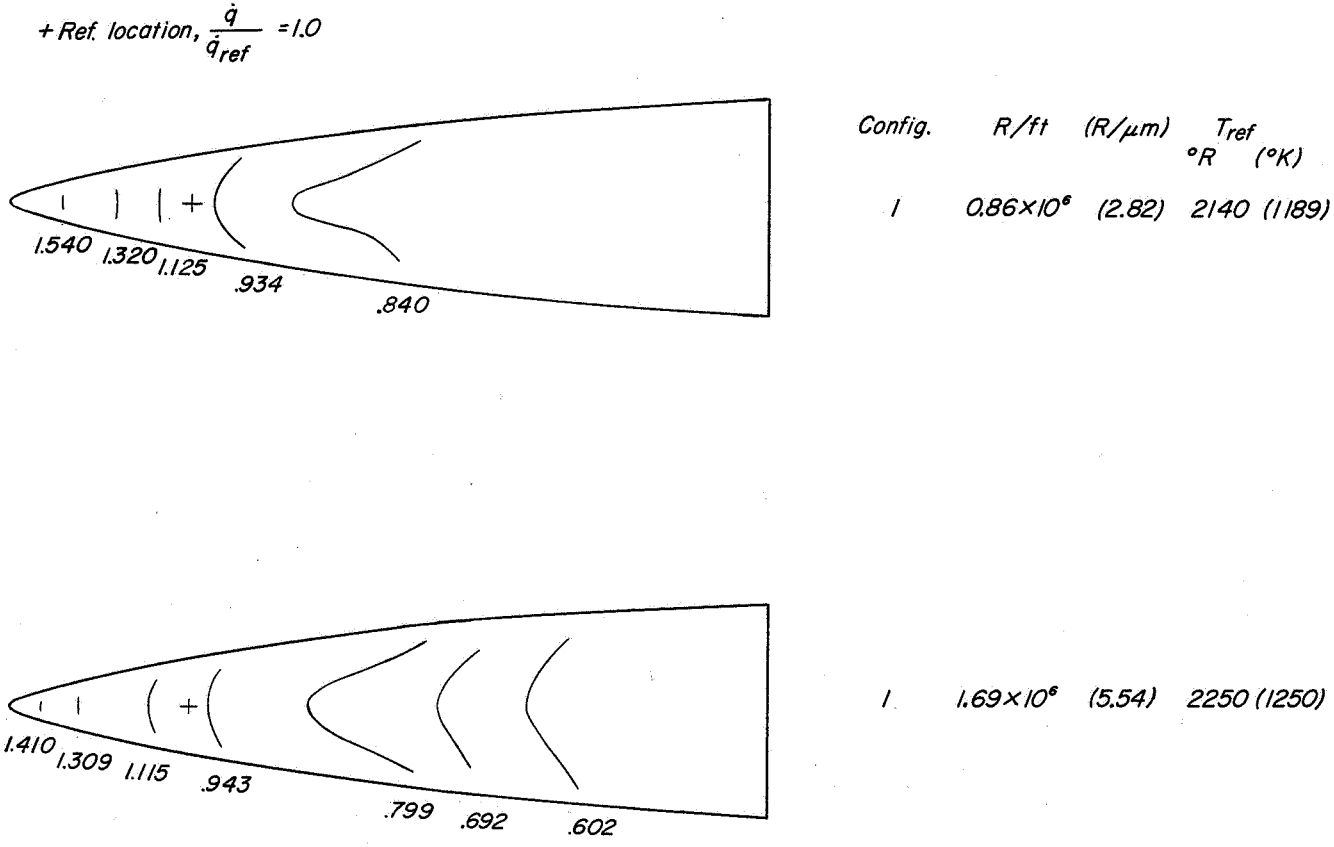

Config.	R/ft	(R/μm)	T_{ref} °R	(T_{ref} °K)
1	0.86×10^6	(2.82)	2140	(1189)
1	1.69×10^6	(5.54)	2250	(1250)

(a) Effect of Reynolds number. Bottom view; $\alpha = 15^0$; $\Lambda = 90^0$; tail off.

Figure 3.- Nondimensional heating contours, $\frac{\dot{q}}{\dot{q}_{ref}}$, over the surfaces of the variable-geometry reentry-vehicle models.

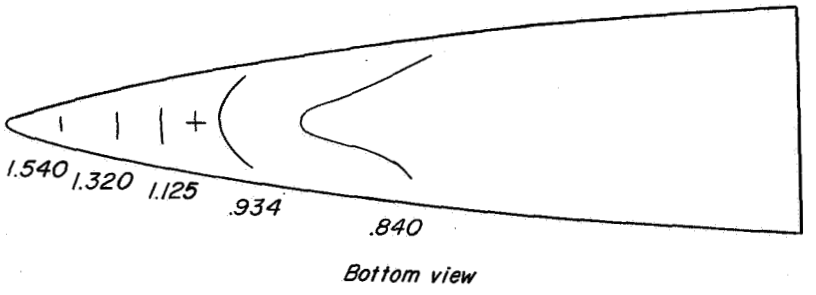

Bottom view

Config.	Nose	T_{ref} °R (°K)
1	Sharp	2140 (1189)

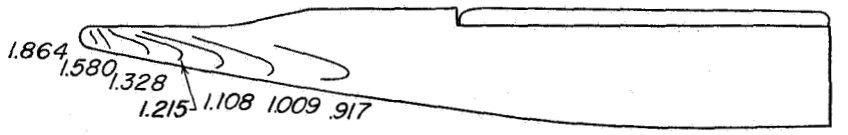

Side view

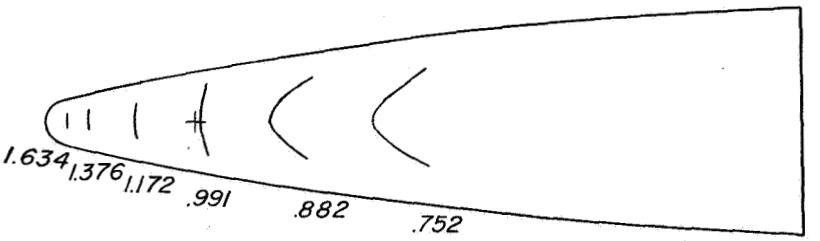

Bottom view

Config.	Nose	T_{ref} °R (°K)
5	Blunt	2105 (1169)

(b) Effects of nose bluntness. $\alpha = 15^0$; $\Lambda = 90^0$; tail off.

Figure 3.- Continued.

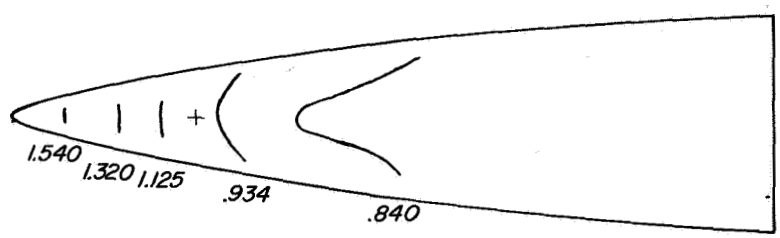

Config.	Tail Γ_h, deg	Tail i_h, deg	T_{ref} °R	T_{ref} (°K)
1	Off		2140	(1189)

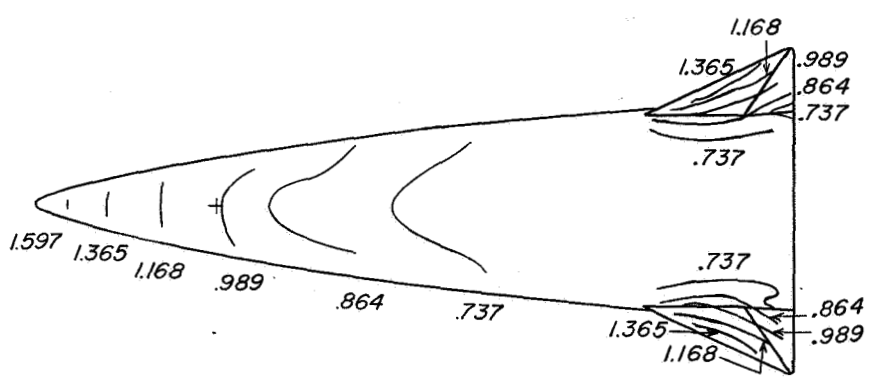

Config.	Tail Γ_h, deg	Tail i_h, deg	T_{ref} °R	T_{ref} (°K)
2	-30	0	2125	(1181)

(c) Tail induced effects. Bottom view; $\Lambda = 90^0$; $\alpha = 15^0$.

Figure 3.- Continued.

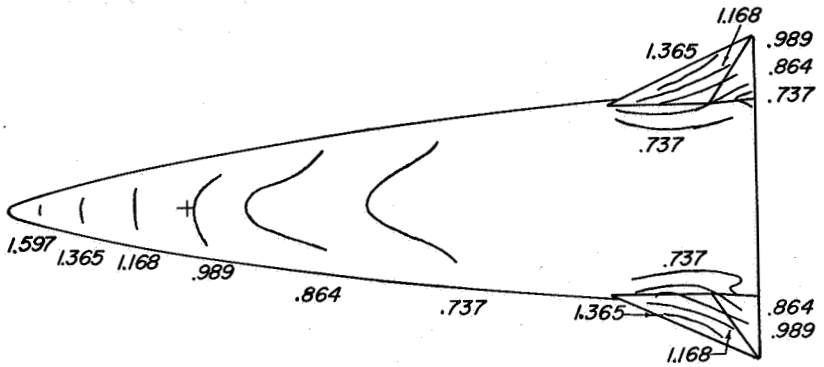

Config.	Tail Γ_h, deg	Tail i_h, deg	T_{ref} °R	T_{ref} (°K)
2	-30	0	2125	(1181)

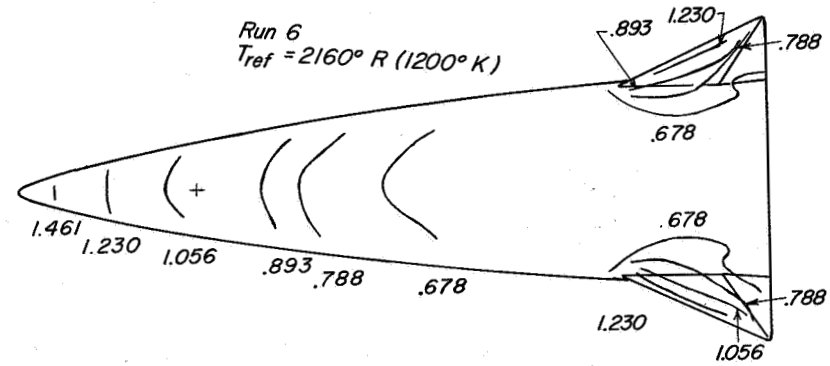

Config.	Tail Γ_h, deg	Tail i_h, deg	T_{ref} °R	T_{ref} (°K)
4	-30	-10	2160	(1200)

(d) Effects of tail incidence. Bottom view; $\Lambda = 90^0$; $\alpha = 15^0$.

Figure 3.- Continued.

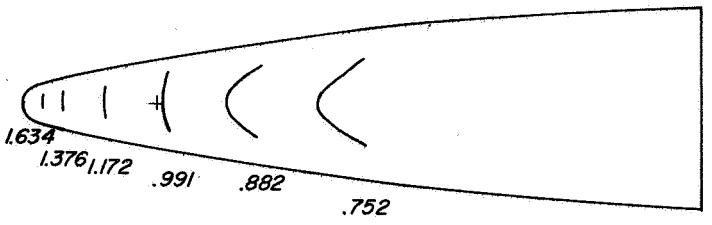

Config.	Wing Λ, deg	Tail Γ_h, deg	Tail i_h, deg	T_{ref} °R (°K)
5	90	Off		2105 (1169)

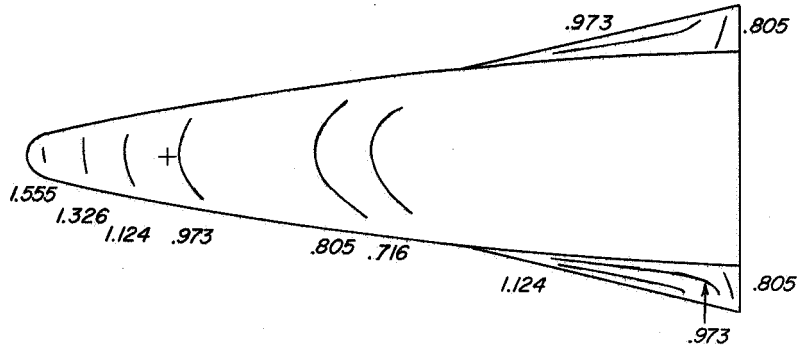

Config.	Wing Λ, deg	Tail Γ_h, deg	Tail i_h, deg	T_{ref} °R (°K)
6	75	Off		2185 (1214)

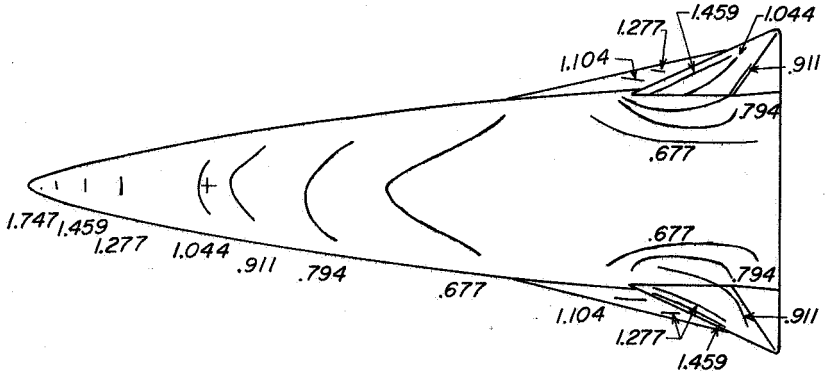

Config.	Wing Λ, deg	Tail Γ_h, deg	Tail i_h, deg	T_{ref} °R (°K)
3	75	-30	0	2160 (1200)

(e) Wing induced effects. Bottom view; $\alpha = 15^{\circ}$.

Figure 3.- Continued.

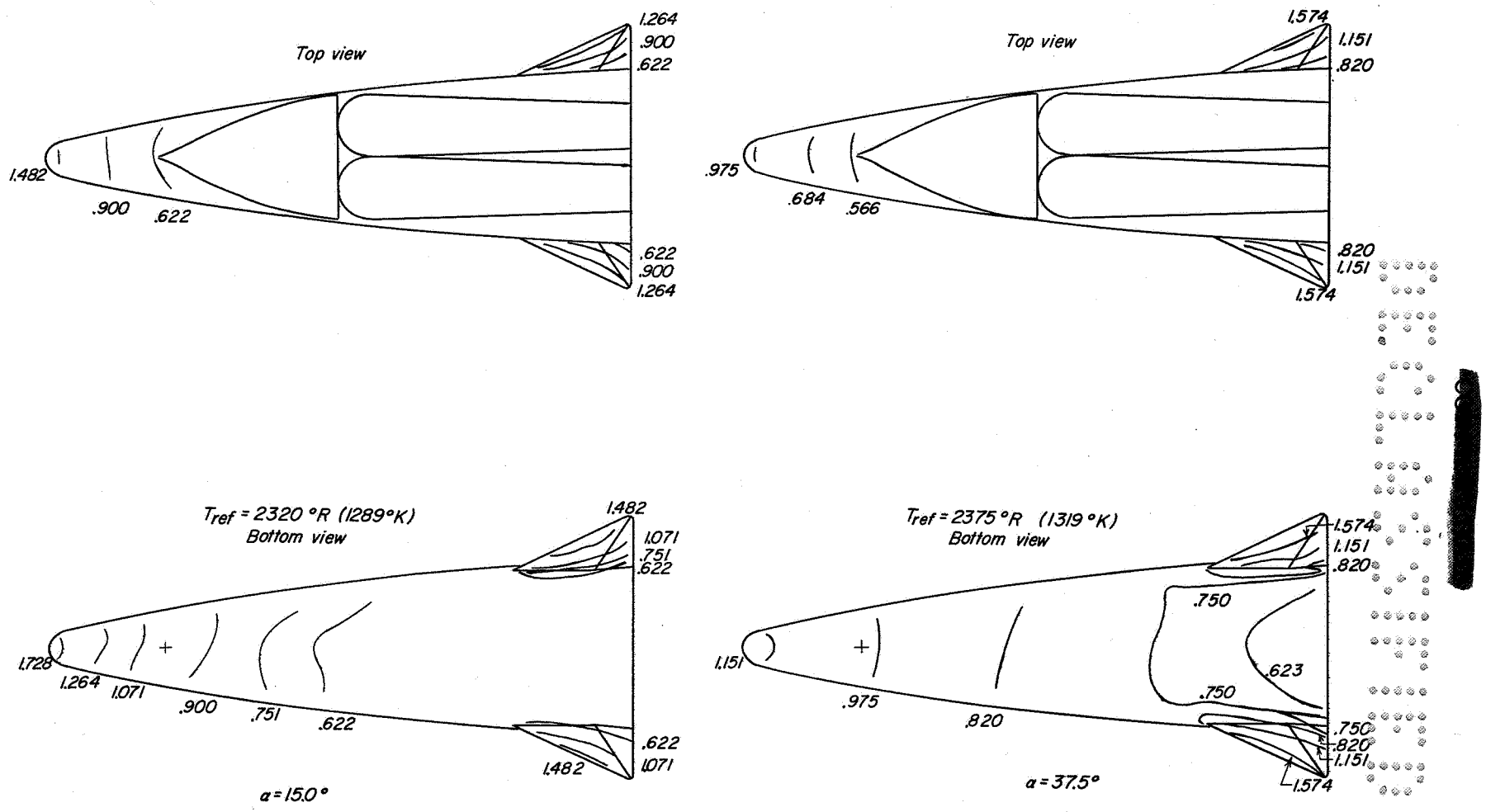

(f) Effect of angle of attack for configuration 7. $\Lambda = 90^0$; $\Gamma_h = -30^0$; $i_h = -10^0$.

Figure 3.- Continued.

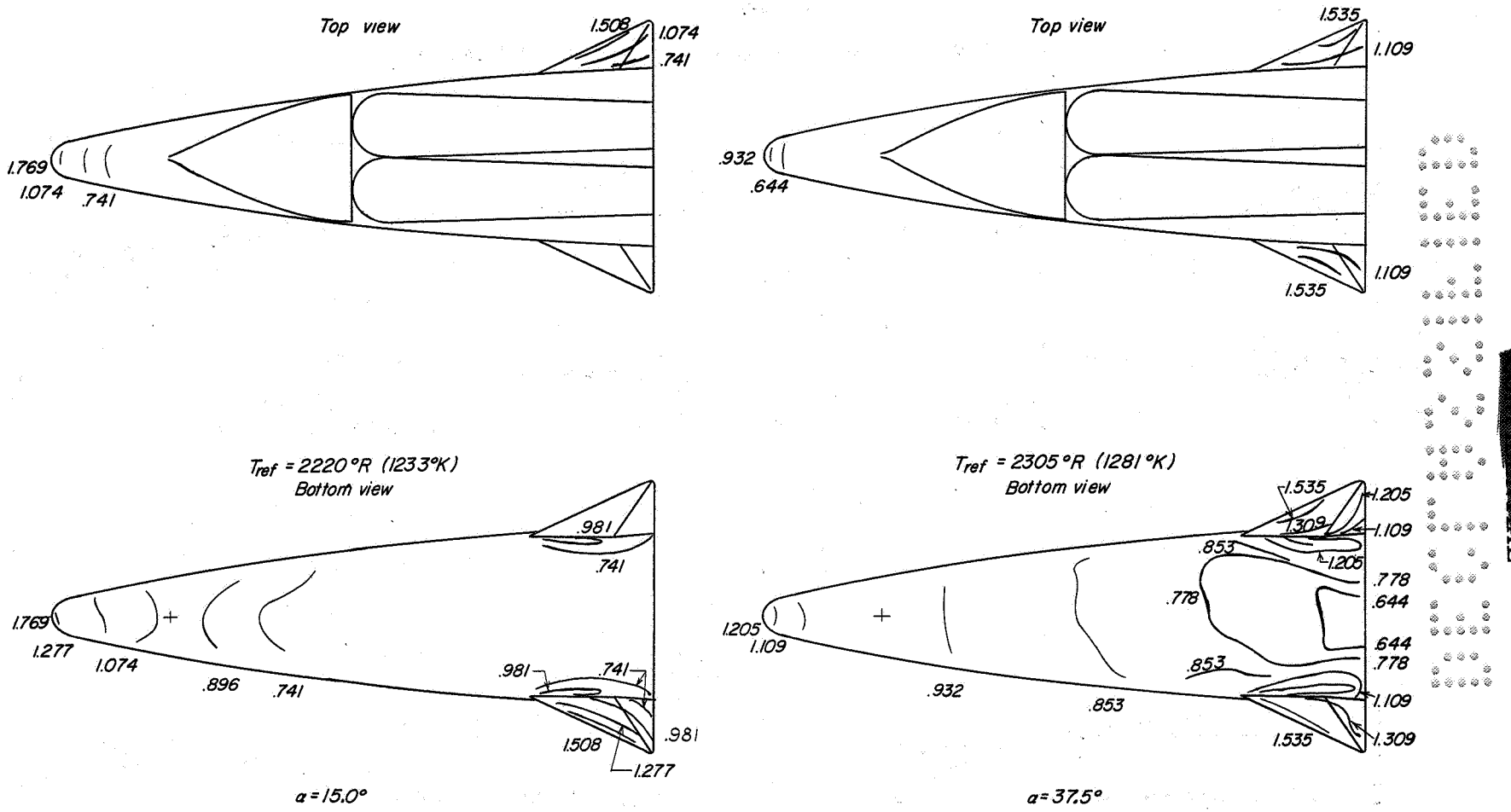

(g) Effect of angle of attack for configuration 8. $\Lambda = 90^0$; $\Gamma_h = -60^0$; $i_h = 0^0$.

Figure 3.- Concluded.

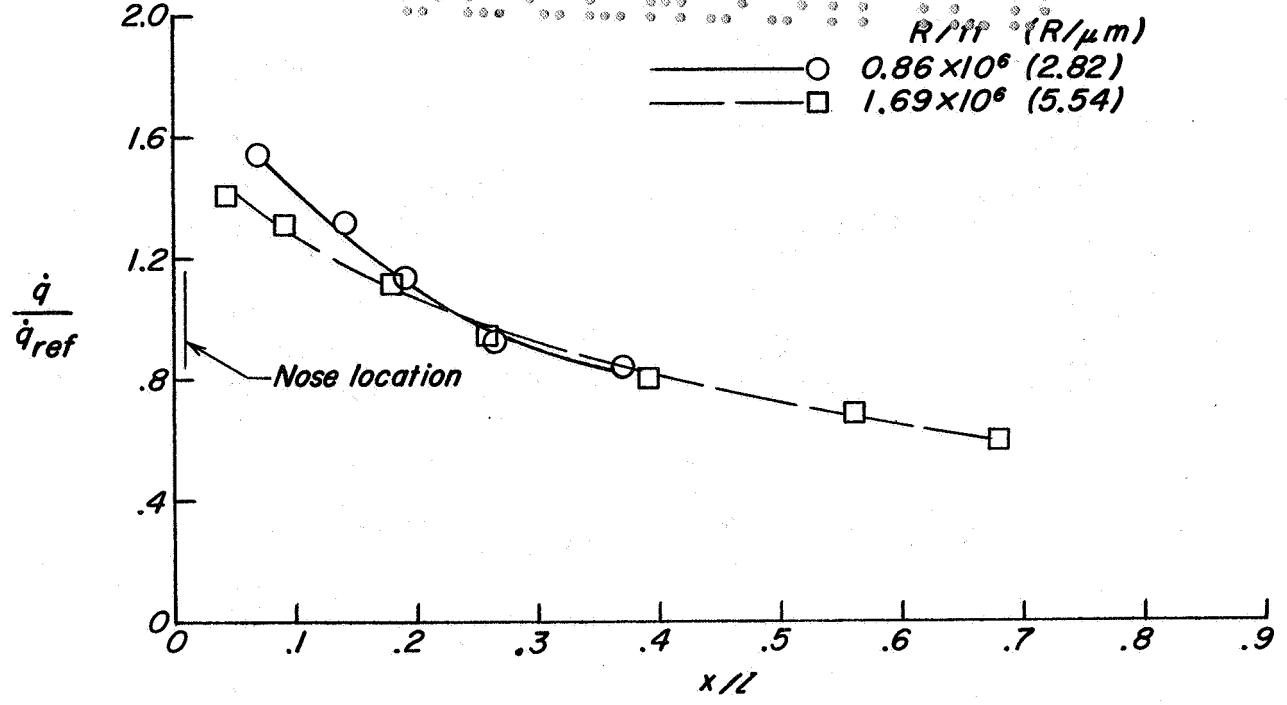

(a) Effect of Reynolds number. Configuration 1; $\alpha = 15^0$.

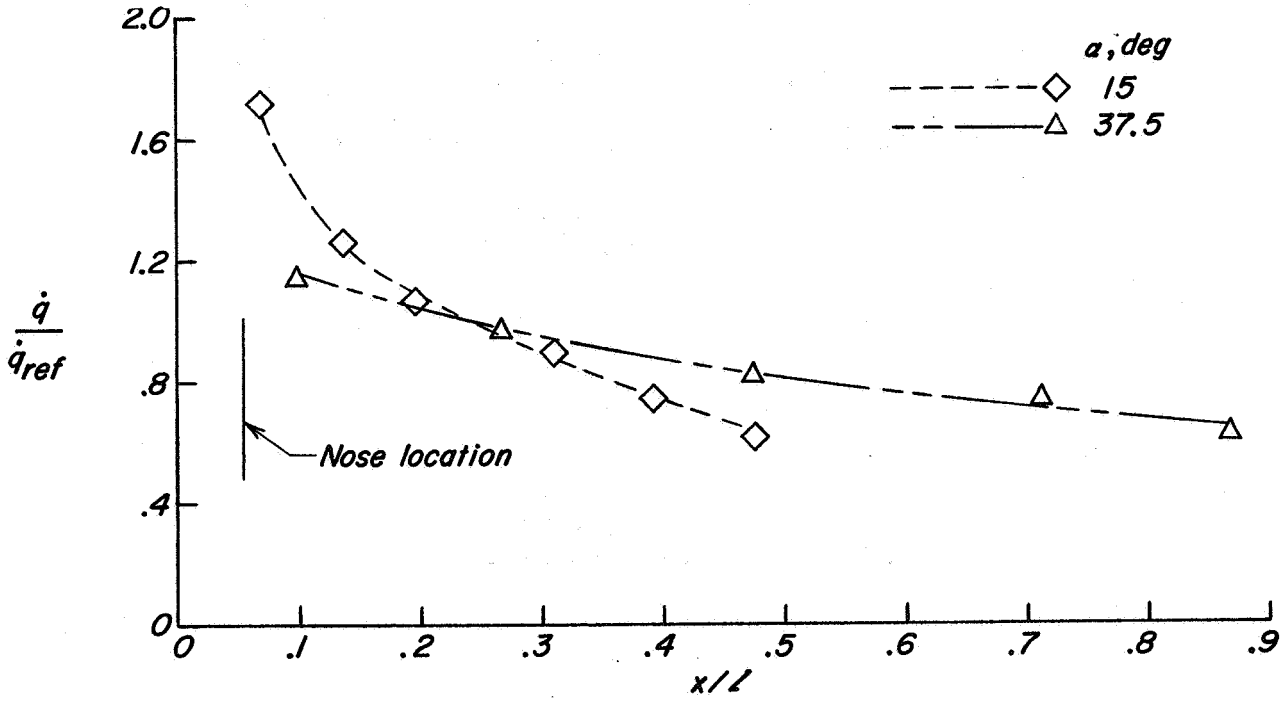

(b) Effect of angle of attack. Configuration 7.

Figure 4.- Nondimensional heating along lower surface center line of models. Reference location is at $x/\ell = 0.24$ (see fig. 1).

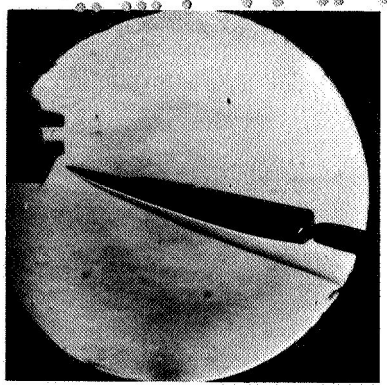

Config. 1

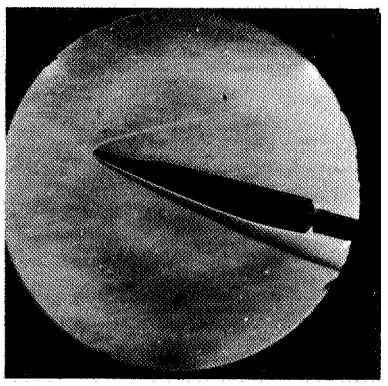

Config. 6

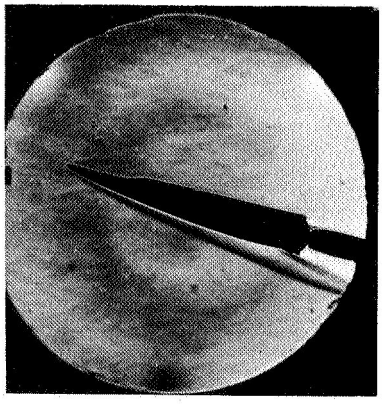

Config. 3

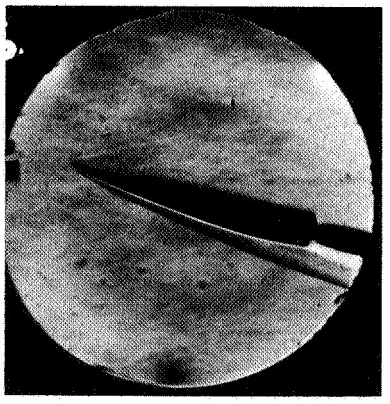

Config. 4

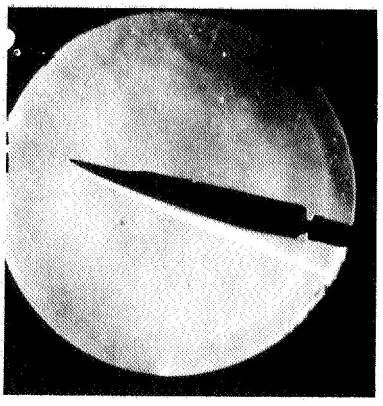

Config. 1
R=1.69 per ft
(5.54 per μm)

(a) Side views. $\alpha = 15^{0}$. L-67-1011

Figure 5.- Schlieren photographs of models of variable-geometry vehicle.

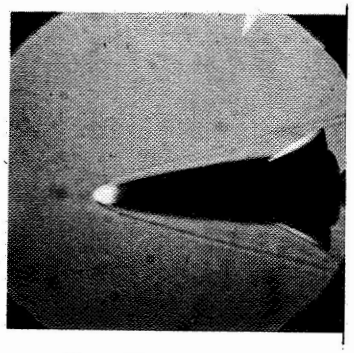

Config. 7
Bottom view
$\alpha = 15°$

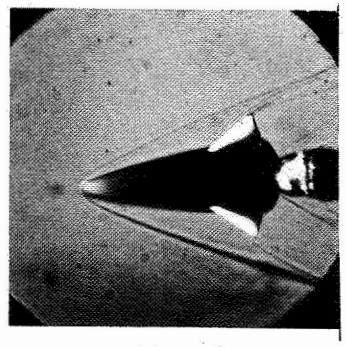

Config. 7
Bottom view
$\alpha = 37.5°$

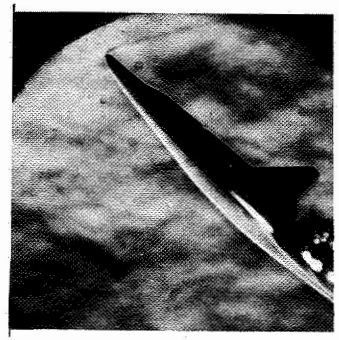

Config. 7
Side view
$\alpha = 37.5°$

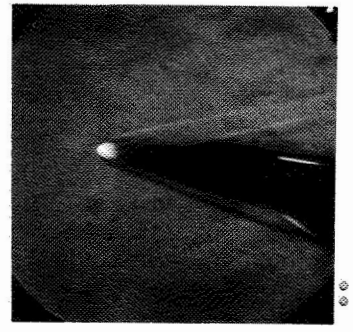

Config. 8
Rolled bottom view
$\alpha = 15°$

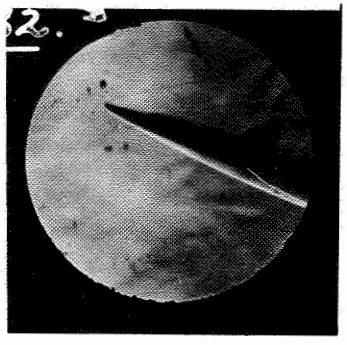

Config. 8
Side view
$\alpha = 15°$

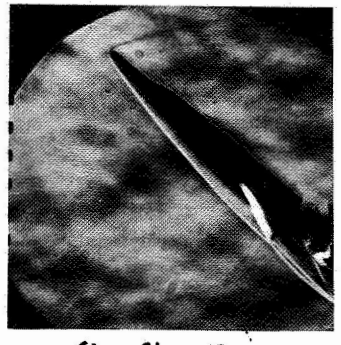

Config. 8
Side view
$\alpha = 37.5°$

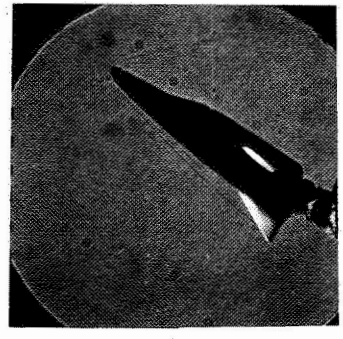

Config. 8
Rolled bottom view
$\alpha = 37.5°$

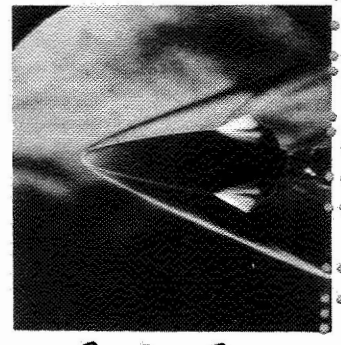

Config. 8
Bottom view
$\alpha = 37.5°$

(b) Configurations 7 and 8.

L-67-1012

Figure 5.- Concluded.

[redacted]

"The aeronautical and space activities of the United States shall be conducted so as to contribute . . . to the expansion of human knowledge of phenomena in the atmosphere and space. The Administration shall provide for the widest practicable and appropriate dissemination of information concerning its activities and the results thereof."

—National Aeronautics and Space Act of 1958

NASA SCIENTIFIC AND TECHNICAL PUBLICATIONS

TECHNICAL REPORTS: Scientific and technical information considered important, complete, and a lasting contribution to existing knowledge.

TECHNICAL NOTES: Information less broad in scope but nevertheless of importance as a contribution to existing knowledge.

TECHNICAL MEMORANDUMS: Information receiving limited distribution because of preliminary data, security classification, or other reasons.

CONTRACTOR REPORTS: Scientific and technical information generated under a NASA contract or grant and considered an important contribution to existing knowledge.

TECHNICAL TRANSLATIONS: Information published in a foreign language considered to merit NASA distribution in English.

SPECIAL PUBLICATIONS: Information derived from or of value to NASA activities. Publications include conference proceedings, monographs, data compilations, handbooks, sourcebooks, and special bibliographies.

TECHNOLOGY UTILIZATION PUBLICATIONS: Information on technology used by NASA that may be of particular interest in commercial and other non-aerospace applications. Publications include Tech Briefs, Technology Utilization Reports and Notes, and Technology Surveys.

Details on the availability of these publications may be obtained from:

SCIENTIFIC AND TECHNICAL INFORMATION DIVISION

NATIONAL AERONAUTICS AND SPACE ADMINISTRATION

Washington, D.C. 20546

[redacted]